Spin–orbit-interaction induced electron spin coherence in slightly hydrogenated graphene within a topological insulating regime

J. Kamijo[1], T. Nakamura[2], T. Kato[1], J. Haruyama[1*]

[1]Faculty of Science and Engineering, Aoyama Gakuin University, 5-10-1 Fuchinobe, Sagamihara, Kanagawa 252-5258, Japan

[2]Institute for Solid State Physics, The Tokyo University, 5-1-5 Kashiwanoha, Kashiwa, Chiba 277-8581, Japan

*****Corresponding author E-mail: J-haru@ee.aoyama.ac.jp (J. H.)

The spin–orbit interaction (SOI) is known to scatter the electron spin, causing spin flipping in thin metals, semiconductor two-dimensional (2D) electron gases, and carbon nanotubes. Thus, the introduction of SOI tends to eliminate the specific advantage of graphene for spintronics, which can retain spin coherence stronger than other 2D materials due to absent SOI. Here, we report that the SOI can induce preservation of spin coherence in interference phenomena of electron waves, by detecting the non-local resistance in 0.06 %-hydrogenated graphene within a diffusive carrier transport regime. The present observation of a SOI-induced strong spin coherence in slightly hydrogenated graphene opens the door to novel carbon spintronics manifested by spin interference as a topological insulator, as well as graphene edge spintronics.

The small mass of carbon atoms has prevented experimental introduction of intrinsic spin–orbit interaction (SOI), which produces various interesting phenomena (such as topological insulating states and the spin Hall effect (SHE)[1-6]), in graphene. However, it was recently reported that the controlled addition of small amounts of covalently bonded hydrogen atoms can introduce a colossal enhancement of the SOI due to out-of-plane symmetry breaking (the so-called Rashba-type SOI), resulting in a SHE[7,8].

Phase interference phenomenon of electron spin waves is one of attractive quantum effects, also highly valuable for spintronics (supplementary information (SI) (1))[11-17,26]. Recent theories suggest a unique feature of graphene, in which SOI may not necessarily cause spin flipping that changes the weak localization (WL, a constructive phase interference between partial electron waves encircling graphene in opposite directions along time-reversal symmetry paths)[11-17,26] to anti-localization (AL, destructive phase interference) through a π phase shift[9,10]. SOI changes the WL to AL only when the out-of-plane mirror symmetry for SOI is broken[9] and also Berry phase β satisfies $\beta/\pi > 0.5$[10], as is the case for other conventional 2D materials. For symmetric SOI systems (e.g., graphene) and for $\beta/\pi < 0.5$, SOI leads to just induced suppression of decoherence in the WL correction, which can be taken as saturation of phase relaxation time $\tau_\phi(T)$ as the temperature (T) approaches zero. Thus, in graphene, SOI tends to preserve spin coherence at lower temperatures and with an applied perpendicular magnetic field (B). In both cases, coupling of the SOI with an in-plane Zeeman effect can also reduce this SOI-induced decoherence suppression through sp^3 hybridization by asymmetrically deposited impurities. These theories imply that the SOI induces preservation of spin coherence and, subsequently, spin phase interference phenomena in topological insulating graphene, which is highly important for future spintronic devices[18,19] using electron spin waves controlled by applied electric fields as well as graphene edge spintronics[20-25]. Nevertheless, so far no experimental work has been carried out to assess the above theories.

The present work represents the first experimental proof of their validity. We reveal that the phase interference of electron waves yields three R_{NL} peaks, which arise from WL appearing only at specified back gate voltages (V_{bg}) to form the WL interference paths due to spin accumulation through the SHE. The phase destruction (decoherence) in WL is significantly suppressed by the introduced strong SOI (with SO relaxation length L_{so} as small as ~40 nm), thus resulting in enhanced preservation of spin coherence without spin flipping, indicating out-of-plane SOI symmetry as a unique property of graphene[9,10]. This SOI-induced suppression of decoherence is also linearly reduced by coupling with the in-plane Zeeman effect[9]. The loop-like phase interference paths for

WL may be retained even at applied high perpendicular B, resulting in Altshuler-Aronov-Spivak (AAS) oscillations (with n-times-encircling electron wave paths), which are conventionally observed only in cylindrical structures like a carbon nanotube (CNT) (SI (1))[14-17,26], in the present hydrogenated (H)-graphene.

In the present experiments, the exact electron beam (EB) dose irradiated to the hydrogen silsesquioxane (HSQ) resist ($(HSiO_{3/2})_n$) on pristine graphene, necessary to achieve an accurate small-volume hydrogenation (<< 1%) of graphene, was optimized following refs. 7 and 25 (SI (2)). An example of change in Raman spectrum before and after HSQ treatment is shown in Figs. 1A and 1B, respectively. The hydrogenation volume (N_H) estimated from the D/G ratios is linearly proportional to the EB dose (Fig. 1C). In order to introduce $N_H \sim 0.06\%$ and an SOI similar to the largest value reported in ref. 7 with limited disorder giving the present diffusive electron transport (SI (2)), we employed an EB dose of 50 mC/cm^2. Figures 1D and 1E show an optical microscope image and a schematic view of the four-probe electrode pattern to detect phase interference phenomena of spin electron waves as change in R_{NL} for H-graphene, respectively.

Three R_{NL} peaks around $V_{bg} \sim 13$, 22, and 28 V for $N_H = 0.06\%$ are apparent in Fig. 2A. Because these are non-local measurements, the three peaks are associated with SOI and spin current of SHE caused by the V_{bg}. Indeed, these R_{NL} peaks are not approximately observed in pristine graphene (i.e., $N_H = 0$ % in Fig. 2A). Only a very small R_{NL} peak due to ohmic contribution is observable around $V_{bg} \sim 14$V[7]. The broad peak at $V_{bg} \sim 13$ V corresponds to the Dirac point (Fig. 2A, inset), in qualitative agreement with the previous observation of R_{NL} arising from SOI in graphene hydrogenated by HSQ treatment[7]. In contrast, the other two R_{NL} peaks above the Dirac point were not observed both in previous[7] and in our present H-graphene with a conventional Hall bar pattern. Thus, the two additional peaks are unique to the four-probe pattern measurement. As mentioned for Fig. 1E, the spin current due to SHE accumulates around electrodes 1 and 2 in the present four-probe pattern, resulting in the induced emergence of electron spin phase interference. Hence, at least these two R_{NL} peaks should be strongly correlated to phase interference among the accumulated electron spins.

In Fig. 2B, negative magnetoresistances (MRs) (i.e., a decrease in the MR with increasing B) are observed around all three R_{NL} peaks at $T = 1.5$ K, when an in-plane B is applied. Negative MR with an applied in-plane B is conventionally considered an evidence of SOI[7]. Ref. 7 reported that negative MRs with an oscillatory behaviour at the R_{NL} peaks in an in-plane-B range linked to the Larmor spin precession frequency ($\omega_B = \Gamma \Delta B \leq D_s/W^2$, where Γ is the gyromagnetic ratio, W is the width of the sample and D_s is the spin diffusion coefficient) could represent a strong evidence for the presence of SOI and SHE. However, the trend of the negative MR in Fig. 2B is very different from that in ref. 7. For V_{bg} between 13 and 16 V (corresponding to the $n = 1$ R_{NL} peak in Fig. 2A), the negative MR is linear, with no oscillations. For V_{bg} = 21, 22, or 28 V (the $n = 2$ or $n = 3$ R_{NL} peaks), an oscillatory-like behaviour emerges, with a period of $\Delta B \sim 4$ T, which is only half the ΔB range of 8 T reported in ref. 7. In the latter work, $\mu \sim 20{,}000$ cm^{2}V^{-1}s^{-1} and $W = 1$ μm were employed to fit the oscillating signal in a ΔB range of ~ 8 T and obtained the best fit ($D_s \propto \mu$). In contrast, our diffusive samples have low μ (< ~10,000 cm^{2}V^{-1}s^{-1}) and $W = 4$ μm, leading to a D_s/W^2 value 30 times smaller than that in ref. 7. Thus, the present ΔB range of ~ 4 T cannot satisfy the condition $\omega_B = \Gamma \Delta B \leq D_s/W^2$, assuming similar Γ values, and cannot be interpreted in terms of Larmor spin precession. Consequently, the Larmor spin precession is not the dominant factor in the negative MRs of Fig. 2B, and we cannot confirm the presence of SOI based on this result.

In order to clarify the origin of the three R_{NL} peaks, which should have a strong correlation with the SOI-based spin phase interference, we measured the semi-logarithmic temperature dependence of the corresponding non-local conductance (G_{NL}) values (i.e., the inverse of the three R_{NL} peak values). The results in Fig. 3A highlight a linear relationship at high temperatures (above ~ 6 K), whereas G_{NL} saturates below ~ 6 K. These results are in good qualitative agreement with those observed for WL in CNTs[11], 2DEG, and thin metal films, suggesting that the three R_{NL} peaks in Fig. 2A can be attributed not only to the SHE, but also to the WL. The results actually prove the presence of the loop-like constructive spin phase interference paths between two partial waves encircling H-graphene in opposite directions (Fig. 1E). Thus, our samples are within the diffusive electron transport regime. This suggest that the two R_{NL} peaks at 22 and 28 V, above the Dirac point, appear

only when the accumulated spin density arising from the SHE satisfies the optimal values to create the constructive interference loop-path for WL in H-graphene. The origin of this effect is also discussed later on, from the viewpoint of electron waves encircling H-graphene *n*-times (Fig. 3B).

The best fitting to the linear-temperature dependence at high temperatures by WL formula in Eq. (1)[11] gives $p = 4$ for $W = 4$ μm and $L = 24$ μm for the present H-graphene.

$$G(T) = G_o + \frac{e^2}{2\pi^2\hbar}\frac{W}{L}\ln\left[1+\left(\frac{T}{T_c(B,\tau_s)}\right)^p\right] \qquad (1)$$

The fitted p value suggests decoherence of the spin phase interference by electron–electron interactions, as in multi-walled CNTs[11]. In contrast, the critical temperature (T_c) of ~ 6 K for the low-temperature saturation at $B = 0$ T is much higher than that observed in CNTs (e.g., $T_c = 0.3$ K for $B = 0$ T[11]). In conventional 2D materials, phase relaxation length, $L_\phi(T) = \sqrt{D\tau_\phi}$ is given by $\tau_\phi^{-1}(T) = \tau_{in}^{-1}(T) + 2\tau_s^{-1}$, where D is the diffusion constant and τ_ϕ, τ_{in}, and τ_s are the relaxation times for the phase coherence and inelastic and magnetic spin scattering, respectively. At $T > T_c$ for $\tau_{in}(T)^{-1} >> \tau_s^{-1}$, the decoherence is governed by inelastic scattering factors reflected in the p value, whereas at $T < T_c$ for $\tau_{in}(T)^{-1} << \tau_s^{-1}$, magnetic spin scattering (which is mostly independent of the temperature) dominates the decoherence, leading to its saturation at high temperature. A T_c as high as ~ 6 K suggests the presence of a larger τ_s^{-1} rate. On the other hand, our graphene samples, which were mechanically exfoliated from graphite, contain no magnetic impurities, and the three R_{NL} peaks in Fig. 2A are associated with spin currents arising from SOI. Thus, the high T_c can originate from the SO scattering rate τ_{so}^{-1}, rather than from τ_s^{-1}. The SOI-induced saturation (i.e., induced suppression) of decoherence in the WL agrees qualitatively with the theoretical prediction for out-of-plane symmetric SOI in graphene mentioned above[9,10]. Moreover the presence of only the positive conductance also supports the theory that the SOI causes no spin flipping, thus resulting in no change of WL to AL. This is also consistent with the suggestion of a preserved out-of-plane SOI symmetry in H-graphene[9].

The perpendicularly applied B also contributes to the decoherence of the interference effects when the Landau orbit size, $L_B = \sqrt{\hbar/eB}$, becomes smaller than $L_\phi(T)$. For a sufficiently high magnetic field, i.e., when $L_B << L_{so} = \sqrt{D\tau_{so}}$ (where L_{so} is the SOI length), the applied B dominates the saturation of the conductance at lower temperatures. This is consistent with Fig. 3A, which shows a T_c value of ~10 K at $B = 7$ T, much higher than that of ~ 6 K measured at $B = 0$ T. The increase in T_c from 6 K to 10 K under an applied B of 7 T entails a small L_s and a very high SO scattering rate (τ_{so}^{-1}) in the present graphene. T_c corresponds to the temperature for which $L_{in} \approx L_{so}$ at low B, and to the temperature for which $L_{in} \approx L_B$ at high B. At $B = 7$ T, this gives $L_B \approx L_{in} \sim 10$ nm at $T_c \sim 10$ K. Because L_{in} is proportional to $T^{-p/2}$, $L_{in} \approx L_{so}$ becomes ~ 40 nm at $T = T_c \sim 6$ K for $p = 4$ at $B = 0$ T. This L_{so} value is much smaller than the $L_s \sim 1$ μm reported in ref. 7 for $N_H = 0.05\%$ (SI (3)).

Applying B perpendicularly to the graphene plane directly causes decoherence and confirms the abovementioned SOI-induced suppression of decoherence in WL and the absence of spin flipping and AL. With a perpendicular B, negative MRs for the three R_{NL} peaks are observed around $B = 0$ at T = 1.5 K (Fig. 3B), which is within the low temperature regime ($< T_c = 6$ K) for the decoherence saturation by SOI. Because the application of a perpendicular B conventionally leads to decoherence in the spin phase interference, the negative MR indicates presence of WL (i.e., absence of spin flipping and AL) under SOI, consistent with Fig. 3A. Importantly, these negative MRs are observed for the three R_{NL} peaks, but they are not observed for the other V_{bg}'s. This strongly supports the argument that the three R_{NL} peaks only appear at specified V_{bg}, for which the accumulated spin densities satisfy the conditions required to form constructive phase interference paths for the WL.

Based on Fig. 3A, the SOI should suppress the decoherence of the WL under an applied perpendicular B. Indeed, the black dotted curve in Fig. 3C, which is a fit of the data by the theory for SOI-suppressed decoherence, using L_{so} as small as ~ 40 nm as obtained from Fig. 3A, shows reasonably good agreement with the experimental results (SI (4)). In contrast, the blue dotted curve

obtained using L_{so} ~ 4 μm (Fig. 3C), representing an extremely small SOI, exhibits a much sharper trend and does not agree with the experiment. These results thus strongly support the suppression of decoherence in WL by SOI, explained above[10]. Consequently, the observed negative MRs under an applied perpendicular B (Fig. 3B) are consistent with the trends observed for the temperature dependence (Fig. 3A).

The linear slopes of the negative MRs at the three R_{NL} peaks (Fig.2B), which could not be explained by Larmor spin precession, can now be understood based on the reduction of the SOI-induced suppression of decoherence in WL in R_{NL} peaks at B = 0 on applied in-plane B, as follows. An applied in-plane B conventionally causes no decoherence in spin phase interference and should lead to no MR changes. On the other hand, ref. 9 predicted that the SOI-induced suppression of the decoherence in WL can be reduced by a decrease in SOI, due to its coupling with in-plane Zeeman effect, which depends linearly on the in-plane B. In our samples, the decoherence is suppressed even at B = 0 and T < 6 K (Fig. 3A). Thus, the MR values given by SOI-suppressed decoherence at B = 0 at T = 1.5 K linearly decrease by the decoherence recovered through the increase in in-plane B, resulting in the observed negative MRs with linear slope. The red dotted lines in Fig. 2B fitted to the experimental data based on this theory[9]. The excellent fit implies that the linear dependence on in-plane B of the negative MRs at the first R_{NL} peaks (i.e., n = 1, V_{bg} = 13 – 16 V) exactly reproduces that predicted by the theory. This unambiguously proves that the first R_{NL} peak in Fig. 2A originates from the SOI, and hence it is a result of the SHE.

The negative MR at the second and third R_{NL} peaks (i.e., n = 2 and 3 for V_{bg} = 21, 22, and 28 V, respectively) can be also fit by straight lines within approximately ± 2 – 3 T of in-plane B. In this case, however, the slope of the negative MRs are larger than those of the n = 1 R_{NL} peaks, entailing a stronger coupling between SOI and in-plane Zeeman effect compared to those for the n = 1 R_{NL} peak. The reason for this behaviour is discussed in the next part.

In the analysis above, we focused on the negative MRs around B = 0 in Fig. 3B. In contrast, when a higher B is considered for ±5T in Fig. 3B, evident periodic MR oscillations are present, also limited only to the three R_{NL} peaks. These oscillations can be well fitted by the theory of AAS oscillations with a constant normalised period $\Delta B \propto (1/2)(h/e)$ where h is the Planck's constant and e is the elemental charge of electron (SI (4)). The AAS oscillations arise from the modulation of the vector potential confined within an inner cylindrical region (that originates from phase interference paths between partial waves encircling along a cylinder in opposite direction, like those for WL) by penetrating magnetic flux[12-17]. Thus, this result appears extremely anomalous, because such interference paths should be eliminated at high B and AAS oscillations should not be observed in 2D structures, graphene, although the present graphene has similar phase interference loop paths for the WL. Therefore, the fact that we still observe AAS oscillations might suggest that decoherence in the loop paths for WL is strongly suppressed by SOI, and therefore in the present H-graphene the loop paths do not disappear even at perpendicular B as high as ±5T.

Moreover, we find that the oscillation period ΔB among the three R_{NL} peaks decreases by half after each V_{bg} increase (ΔB = 8, 4, and 2 T for V_{bg} = 13, 22, and 28 V, respectively; see inset of Fig. 3B). This suggests the presence of the AAS effect, arising from n-times-encircling paths around the AAS loop (n = 1-3; WL loop shown in Fig. 1e)[14], which is characterised by $\Delta B \propto (1/2)^n(h/e)(\pi r^2)^{-1}$ [14], as proven by fitting the data by the AAS theory. Because the AAS loop at V_{bg} = 13 V (corresponding to the Dirac point) is the most stable, the electron spins tend to circulate two- and three-times along the same AAS loop at the other two specified V_{bg}'s (i.e., 22 and 28 V) when a perpendicular B is applied. This can explain the three R_{NL} peaks that only appear at specified V_{bg}'s satisfying conditions appropriate for forming the WL path, and hence the AAS path with n-times encircling electron waves, as in the present case. As mentioned for Fig. 2B, the linear slope values of the negative MRs for the second and third R_{NL} peaks are larger than those for the first R_{NL} peak. This is also consistent with presence of the n-times encircling paths because the in-plane Zeeman effect is coupled with these two- and three-times encircling interference paths at the same time, and thus the SOI-induced suppression of the decoherence is significantly reduced. Moreover, even possible universal conductance fluctuation is observable in the present H-graphene (SI (5))[26].

References and Notes

1. Sinova, J. et al., *Phys. Rev. Lett.* **92** 126603 (2004).
2. Murakami, S., Nagaosa, N. and Zhang, S.C., *Science* **301,** 1348 (2003).
3. Castro Neto, A. H. and Guinea, F., *Phys. Rev. Lett.* **103**, 026804 (2009).
4. Kane, C. L. & Mele, E. J., *Phys. Rev. Lett.* **95**, 146802 (2005).
5. Kane C. L. & Mele, E. J., *Phys. Rev. Lett.* **95**, 226801 (2005).
6. Abanin, D. A., Geim, A. *et al., Science* **332**, 328-330 (2011).
7. Balakrishnan, J., Koon, G. K. W., Jaiswal, M, Castro Neto, A. H. & Özyilmaz, B., *Nature Physics* **9**, 284-287 (2013).
8. Melinda, S. R., Kim, P. *et al., Nano Lett*. **8**, 4597 (2008).
9. McCann E. and Fal'ko, V. I., *Phys. Rev. Lett.* **108**, 166606 (2012).
10. Shan, W.-Y. *et al*., *Phys. Rev.* B **86** 125303 (2012).
11. Langer, L., Bayot, V., Grivei, E. and Issi, J.-P., *Phys. Rev. Lett.* **76**, 479 (1996).
12. She, S. H. *et al*., *Phys. Rev. Lett.* **84**, 4441 (2000).
13. Song S.N. *et al.*, *Phys. Rev. Lett.* **72**, 697 (1994).
14. Bachtold A. *et al.*, *Nature* (London) **397**, 673 (1999).
15. Haruyama, J., Takesue, I. and Hasegawa, T., *Phys. Rev.* B **65**, 033402 (2001).
16. Altshuler, B.L. *et al., JETP Lett*. **35**, 588 (1982).
17. Imry, Y., Introduction to mesosopic physics. (Oxford University Press, Oxford 2002)
18. Tombros N. *et al*., *Phys. Rev. Lett.* **101**, 046601 (2008).
19. Tombros, N. *et al.*, *Nature* **448**, 571 (2007).
20. Hashimoto, T., Haruyama, J., Roche, S. *et al.*, In-depth review, *Nature Nanotech* (2014).
21. Tada, K., Hashimoto, T., Haruyama, J., Yang, H. & Chshiev, M. S, *Physica Status Solidi B* **249**, 2491-2496 (2012).
22. Shimizu, T., Nakamura, J., Tada, K., Yagi, Y. & Haruyama, J., *Appl. Phys. Lett.* **100**, 023104 (2012).
23. Hashimoto, T., Kamikawa, S., Yagi,Y. & Haruyama, J., *Materials Sciences and Applications* **5**, 1-9 (2014).
24. Shimizu, T., Haruyama. J. *et al*., *Nature Nanotech*. **6,** 45-50 (2011).
25. Kato, T., Nakamura, T., Haruyama. J. *et al*., *Appl. Phys. Lett.* **104**, 252410 (2014).
26. Ando. T. et al., Mesoscopic physics and electronics. Nano Science and Technology series (Klitzing v. K. & Weisendanger R.), ISBN 3-540-63587-4 (Springer-Verlag 1998)

27. The authors thank Y. Yagi, M. Yamamoto, S. Tarucha, H. Hibino, K. Sugawara, T. Ando, T. Enoki, M. Koshino, N. Furukawa, H. Kitano, T. Mitsui, B. Ozyilmaz, A. H. Castro Neto, E. McCann, S. Roche, and M. S. Dresselhaus for their technical contribution, fruitful discussions, and encouragement. The work at Aoyama Gakuin was partly supported by a Grant-in-aid for Scientific Research (Basic research A: 24241046) in MEXT and AOARD grant (135049) in U.S. Air Force Office of Scientific Research.

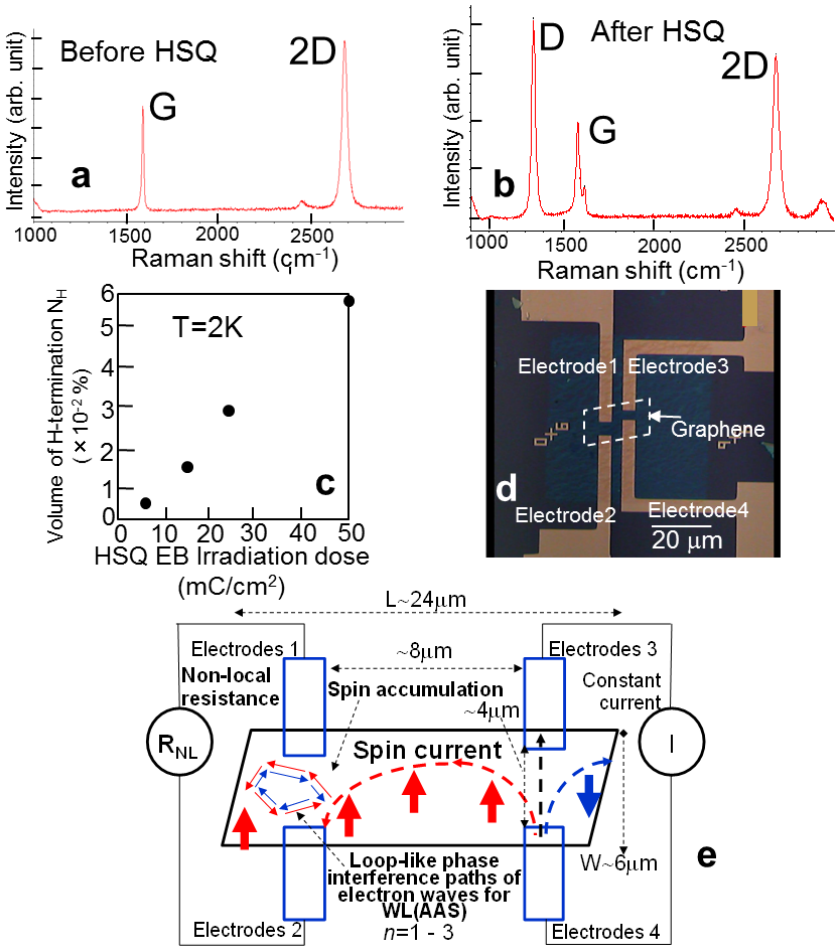

Figure 1
Haruyama et al.

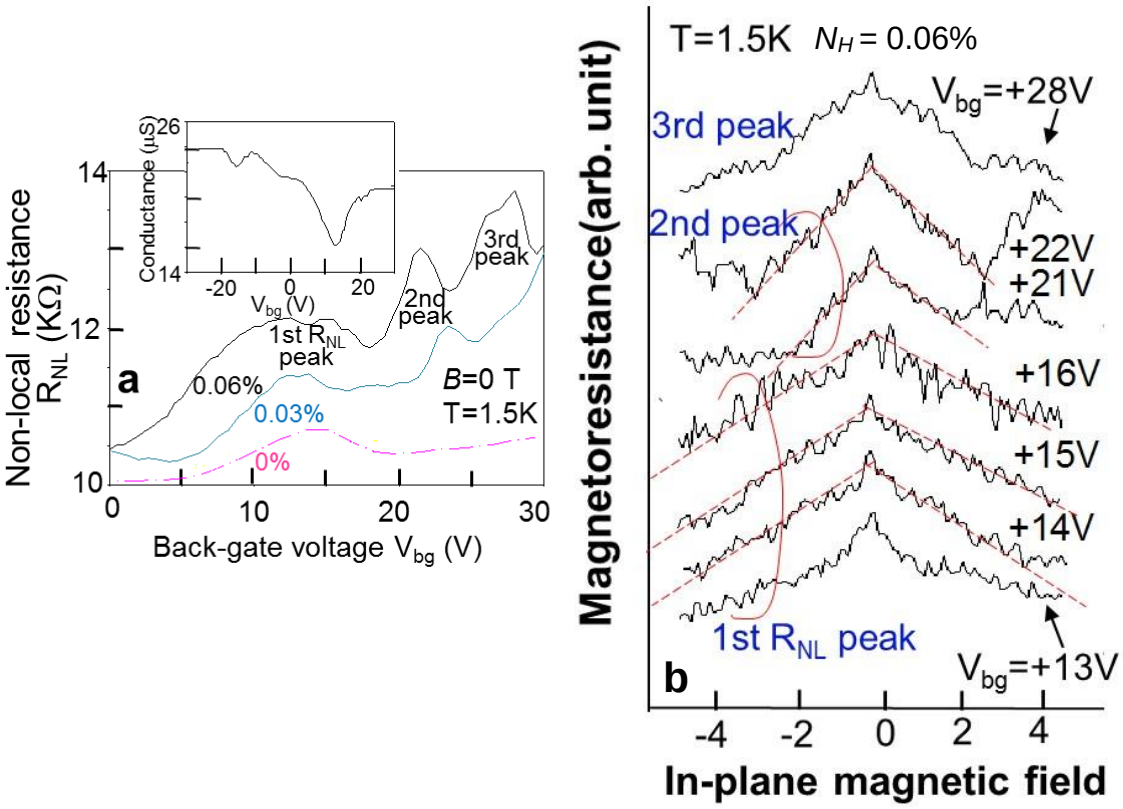

Figure 2
Haruyama et al.

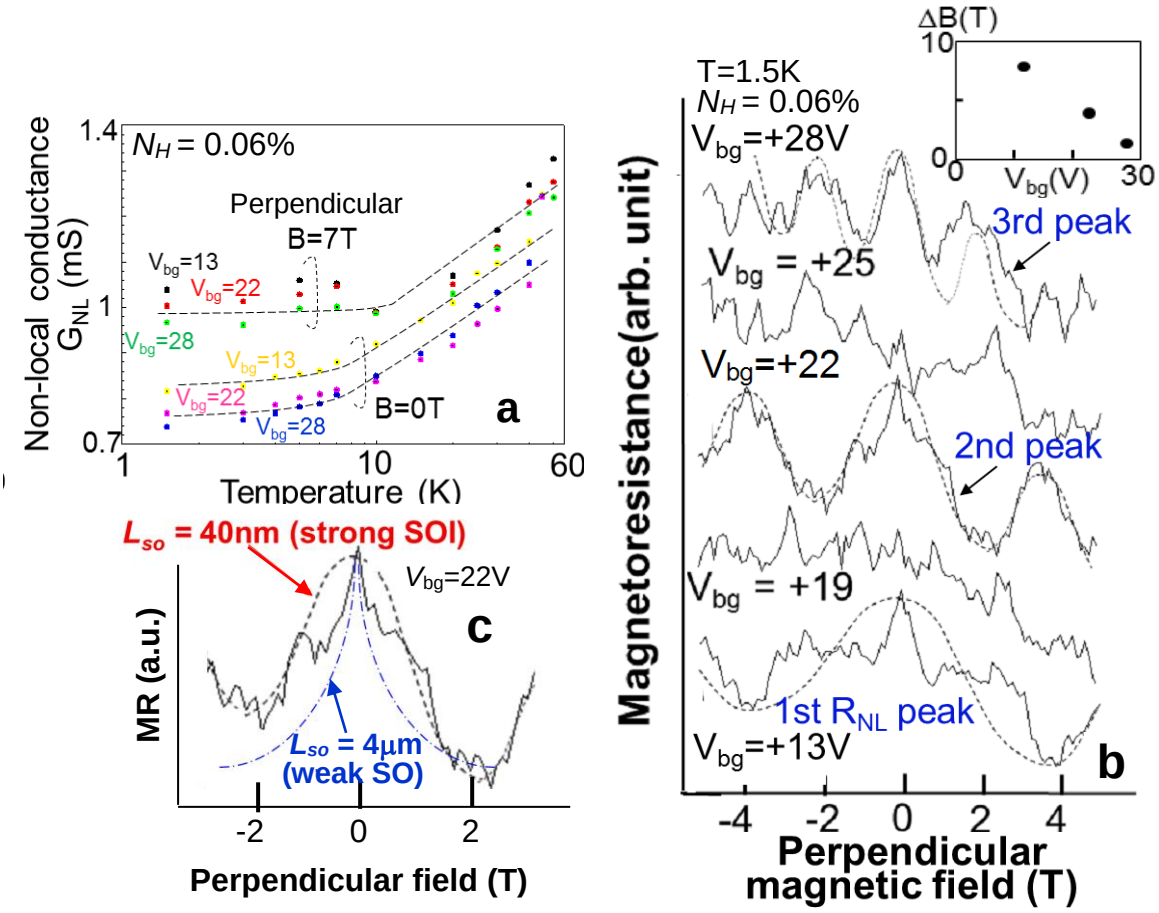

Figure 3
Haruyama et al.

Figure captions

Fig. 1 Sample structures and characterization.
(A)-(B) Examples of Raman spectra of graphene mechanically exfoliated from highly oriented pylolytic graphite before and after HSQ resist treatment. Significantly increased D/G peak ratio in (**B**) suggests hydrogenation of graphene surface.

(C) Volume (area) of hydrogenation (N_H) estimated from D/G peak ratios in the Raman spectrum (like (**A**)) as a function of electron beam (EB) dose to HSQ resist. EB irradiation dose of 50 mC/cm^2, which is employed in the present experiments to give the same N_H (~0.06%) as that in ref. 7, is approximately ten-times larger than EB dose in ref. 7 owing to our EB conditions. It leads to diffusive charge transport regime due to limited disorder in the present graphene with keeping high quality.

(D) Optical microscope image of the four-probe electrode pattern on 0.06%-hydrogenated graphene.

(E) Schematic view of (**D**) with electron spin trajectories for SHE. In contrast to conventional Hall bar, the two electrodes to make main current flow were eliminated. When a constant current flows between electrodes 3 and 4 and a back gate voltage V_{bg} is applied as a perpendicular field, a spin current due to the SHE(SOI) flows towards electrodes 1 and 2, and R_{NL} appears between these electrodes. However, because these spins have no exit channel, they accumulate in the left region of the sample. Spin scattering by the limited disorder introduced by the high EB dose leads to the formation of the loop-like spin phase interference paths of electron waves (with *n*-times encircling) for WL, which are detected as R_{NL} change.

Fig. 2 Non-local resistance (R_{NL}) and its in-plane-magnetic-field(B) dependence.
(A) R_{NL} as a function of V_{bg} and N_H (0, 0.03, and 0.06%) showing evident three peaks around V_{bg} ~ 13, 22, and 28 V (n = 1-3) for N_H ~0.06%. These peaks with Figs. 2B and 3 were attributed to weak localisation (WL) with SOI-induced suppression of phase decoherence of electron waves, and reconfirmed at least in three samples. They were not observed in non-hydrogenated graphenes. Only when the accumulated spin densities satisfy the optimal conditions to form constructive phase interference loop paths for WL (see Fig. 1E) at specified V_{bg}, three R_{NL} peaks are observable. **Inset:** Dirac point.

(B) Negative magnetoresistance (MR) behaviours vs. in-plane B, showing linear slope only around the three R_{NL} peaks in (**a**). MRs at V_{bg} = +13–16 V correspond to the first broad R_{NL} peak at n = 1 in Fig. 2A. MRs at V_{bg} = +21 and +22 V correspond to the second (n = 2), and MR at V_{bg} = +23 V to the third (n = 3) R_{NL} peak, respectively. These peaks cannot be directly explained by Larmor spin precession, unlike for ref. 7. Dotted lines represent data fits by the theory of linear reduction of the SOI-induced decoherence suppression by coupling between SOI and in-plane Zeeman effect[9]. The best fit well explains the linearity, proving presence of SOI-induced suppression of phase decoherence at B = 0.

Fig. 3 SOI-based weak localization: Semi-logarithmic temperature dependence of three non-local conductance (G_{NL}) values and perpendicular B dependence of R_{NL}.
(A) Semi-logarithmic temperature dependence of the inverse values of the three R_{NL} peaks (Fig. 2A) at perpendicular B = 0 and 7 T. They exhibit linear relationships at high temperatures ($> T_c$ ~6 K), whereas they saturate below T_c ~6 K suggesting SOI-induced suppression of the high-temperature decoherence. They are well accounted for by the WL theory (Eq. (1)) shown by dashed lines. These behaviours are observed only around these three R_{NL} peaks, suggesting that the accumulated spin densities for these R_{NL} peaks satisfy conditions optimal to form these constructive phase interference paths for WL.

(B) Negative MR behaviours around $B = 0$ for the three R_{NL} peaks (Fig. 2A) with an applied perpendicular B. They are also observed only around the three R_{NL} peaks (i.e., V_{bg} = +13, +22, and +28 V), supporting the presence of WL as suggested in (**A**). The periodic MR oscillations at high B region are well described by the dashed curves, representing best fits by AAS theory performed with L_{so} = 40 nm despite 2D structure of graphene (SI (4)). This means SOI-induced preservation of spin coherence even at high B.
Inset: AAS oscillation period ΔB estimated at three different V_{bg} shown in the main panel. Their halving with increasing V_{bg} suggests the presence of n-times (n = 1-3) encircling electron waves along the WL path.

(C) Data fits by the AAS theory to the negative MR around $B = 0$, observed at V_{bg} = +22 V in (**B**), using strong and weak SOI parameters (L_{so}) (SI (4)). The better fit obtained with L_{so} = 40 nm suggests a SOI-induced strong suppression of decoherence and absence of spin flipping (i.e., AL) on a perpendicular B regime, as well as those on temperature regime in (**A**).